High-resolution study of Gamow-Teller transitions with the ^{37}Cl(^{3}He, t)^{37}Ar reaction

Y. Shimbara,[1,2,3,*] Y. Fujita,[1,†] T. Adachi,[1,‡] G. P. A. Berg,[2,§] H. Fujimura,[2,‖] H. Fujita,[1] K. Fujita,[2,¶] K. Hara,[2,**] K. Y. Hara,[4,††] K. Hatanaka,[2] J. Kamiya,[2,‡‡] K. Katori,[2] T. Kawabata,[2,§§] K. Nakanishi,[2] G. Martìnez-Pinedo,[5] N. Sakamoto,[2] Y. Sakemi,[2,‖‖] Y. Shimizu,[2,¶¶] Y. Tameshige,[2,***] M. Uchida,[6,†††] M. Yoshifuku,[1] and M. Yosoi[6,‡‡‡]

[1]*Department of Physics, Osaka University, Toyonaka, Osaka 560-0043, Japan*

[2]*Research Center for Nuclear Physics, Osaka University, Ibaraki, Osaka 567-0047, Japan*

[3]*Graduate School of Science and Technology, Niigata University, Nishi-ku, Niigata 950-2012, Japan*

[4]*Department of Physics, Konan University, Higashinada, Kobe 658-8501, Japan*

[5]*Gesellschaft für Schwerionenforschung, D-64291 Darmstadt, Germany*

[6]*Department of Physics, Kyoto University, Sakyo, Kyoto 606-8502, Japan*

(Received 16 April 2012; published 27 August 2012)

Under the assumption of isospin symmetry, $T_z = \pm 3/2 \rightarrow \pm 1/2$ Gamow-Teller (GT) transitions in an isobar quartet with a mass A are analogous, where $T_z = (1/2)(N - Z)$ is the z component of the isospin T. We studied the $T_z = +3/2 \rightarrow +1/2$ GT transitions by the ^{37}Cl(^{3}He, t)^{37}Ar reaction at an incoming beam energy of $E_{\rm beam} =$ 140 MeV/nucleon with an energy resolution of $\Delta E = 30$ keV. The distribution of the GT strength was obtained up to an excitation energy (E_x) of 14.2 MeV. This distribution was compared with that of the $T_z = -2/3 \rightarrow -1/2$ transitions studied in ^{37}Ca β decay up to $E_x = 8.6$ MeV. Although the overall distributions were similar, details of the fine structure were not necessarily reproduced. The experimental results were compared with a shell-model (SM) calculation using the USD interaction and the effective GT operator that compensates for the effect of limited model space. Although the overall distribution was reproduced by the SM calculation, the fragmentation of states was not reproduced. Neutrino cross sections were derived for the ^{8}B solar-neutrino source.

DOI: 10.1103/PhysRevC.86.024312 PACS number(s): 25.55.Kr, 21.10.Hw, 21.60.Cs, 26.65.+t

I. INTRODUCTION

The Gamow-Teller (GT) transition strengths, B(GT), from the ^{37}Cl ground state (g.s.) to the excited states of ^{37}Ar have been studied intensively in connection with ^{37}Cl neutrino detection, where the ^{37}Cl(ν, e^-)^{37}Ar reaction is used to detect solar neutrinos [1–3]. The GT strength is directly obtained by the measurement of β decay. However, the β decay cannot access the ^{37}Cl $\rightarrow$ ^{37}Ar transitions owing to the negative Q value. If the isospin T is a good quantum number, the GT transition strengths are the same in ^{37}Cl $\rightarrow$ ^{37}Ar and ^{37}Ca $\rightarrow$ ^{37}K transitions (see Fig. 1). Therefore, GT transitions from the g.s. of ^{37}Ca to the excited states in ^{37}K have been measured in the ^{37}Ca β decay in order to deduce ^{37}Cl $\rightarrow$ ^{37}Ar transitions. There were several previous studies of ^{37}Ca β decay by detecting the delayed protons from the particle-unbound states of ^{37}K [4–6]. Subsequently, a high-resolution and low-background measurement was performed by Sextro, Gough, and Cerny [7].

The first direct measurement of ^{37}Cl $\rightarrow$ ^{37}Ar GT transitions was performed by Rapaport *et al.* [8] using the ^{37}Cl(p, n)^{37}Ar reaction at $E_p = 160$ MeV with an energy resolution of 300 keV. It is known that at incident beam energies of more than 100 MeV/nucleon and at 0°, charge-exchange (CE) reactions dominantly excite GT transitions. Under these conditions, the differential cross sections in the limit of zero momentum transfer become proportional to B(GT) values [9–14]. By applying the proportionality, they obtained the B(GT) distribution up to an excitation energy E_x of about 12 MeV in ^{37}Ar [8]. The total neutrino cross sections from both the ^{37}Cl(p, n)^{37}Ar reaction and the ^{37}Ca β-decay data gave similar values. Therefore, little attention was paid to the difference of the energy distribution of the B(GT) strength.

Several years later, however, Adelberger and Haxton [15] noticed that there were significant differences between the ^{37}Cl(p, n)^{37}Ar and the ^{37}Ca β-decay data. The strength below

*shimbara@np.gs.niigata-u.ac.jp

†fujita@rcnp.osaka-u.ac.jp

‡Present address: Research Center for Electron Photon Science, Tohoku University, Taihaku-ku, Sendai, Miyagi 982-0826, Japan.

§Present address: Department of Physics and the Joint Institute of Nuclear Astrophysics, University of Notre Dame, Notre Dame, IN 46556, USA.

‖Present address: Liberal Arts and Sciences, Wakayama Medical University, Wakayama 641-8509, Japan.

¶Present address: Department of Physics, Kyushu University, Higashi-ku, Fukuoka 812-8581, Japan.

**Present address: High Energy Accelerator Research Organization, Tsukuba, Ibaraki 305-0801, Japan.

††Present address: Japan Atomic Energy Agency, Tokai, Naka, Ibaraki 319-1195, Japan.

‡‡Present address: Japan Atomic Energy Research Institute, Tokai, Ibaraki 319-1195, Japan.

§§Present address: Department of Physics, Kyoto University, Sakyo, Kyoto 606-8502, Japan.

‖‖Present address: Cyclotron and Radioisotope Center, Tohoku University, Aoba-ku, Sendai, Miyagi 980-8578, Japan.

¶¶Present address: RIKEN, Wako, Saitama 351-0198 Japan.

***Present address: National Institute of Radiological Sciences, Inage-ku, Chiba 263-8555, Japan.

†††Present address: Department of Physics, Tokyo Institute of Technology, Meguro-ku, Tokyo 152-8550, Japan.

‡‡‡Present address: Research Center for Nuclear Physics, Osaka University, Ibaraki, Osaka 567-0047, Japan.

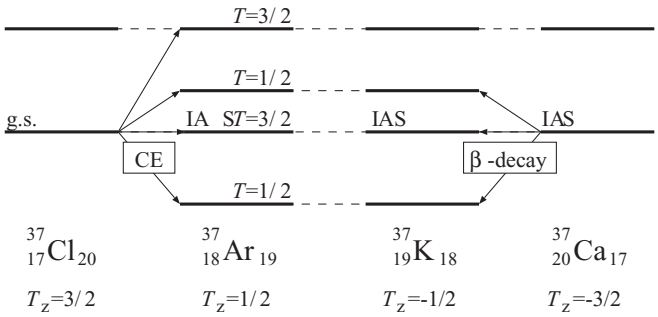

FIG. 1. A schematic view of the isospin symmetry structure and the GT transitions by a charge-exchange reaction and the β decay in the $A = 37$ isobars. The Coulomb displacement energy is subtracted in this figure. Under the assumption of isospin symmetry the transition strength distributions between transitions from the ground state of the $T_z = +3/2$ nucleus to the excited states in the $T_z = +1/2$ nucleus and those from the ground state of the $T_z = -3/2$ nucleus to the excited states in the $T_z = -1/2$ nucleus are the same. ^{37}Cl, ^{37}Ar, ^{37}K, and ^{37}Ca correspond to $T_z = -3/2, -1/2, +1/2$, and $+3/2$, respectively. The transition strengths between $^{37}\mathrm{Cl} \rightarrow {}^{37}\mathrm{Ar}$ and $^{37}\mathrm{Ca} \rightarrow {}^{37}\mathrm{K}$ should have the same distributions in the energy spectra.

$E_x = 4$ MeV deduced from the $^{37}\mathrm{Cl}(p, n)^{37}\mathrm{Ar}$ experiment was only half of that observed by the ^{37}Ca β decay. In addition the strong peaks observed above $E_x = 6.02$ MeV in the (p, n) experiment were not reported at the corresponding excitation energies in β decay. Adelberger and Haxton concluded that these discrepancies were caused by the analysis of the ^{37}Ca β-decay data under the unreasonable assumption that all delayed protons from ^{37}K levels decayed to the g.s. of ^{36}Ar [15].

García *et al.* [16] measured protons following ^{37}Ca β decay with a better resolution of 16 keV. The p-γ coincidence measurement allowed proton decays feeding the g.s. of ^{36}Ar to be distinguished from those feeding the excited states of ^{36}Ar. In their studies a larger B(GT) strength appeared above 6 MeV. However, still noticeable differences remained, and these could not be explained by the asymmetry of the isospin. Subsequently, the assumption in the analysis that all proton-unbound daughter states in ^{37}K decayed by proton emission was questioned. The studies of $^{36}\mathrm{Ca}(p, \gamma)^{37}\mathrm{K}$ [17] and $^{40}\mathrm{Ca}(p, \alpha)^{40}\mathrm{K}$ [18] reactions suggested that a few proton-unbound states in ^{37}K above the proton separation energy had significant probabilities of undergoing γ decay. Actually recalculation of the B(GT) distribution by taking both the delayed proton emission and the γ decay into account reduced a large part of the difference [19,20].

In order to study further differences, a transition-by-transition comparison is necessary. In ^{37}Ca β decay, individual GT strengths were obtained up to $E_x = 8.5$ MeV in ^{37}K [16,20]. Unfortunately, only a few GT transitions were resolved above $E_x = 4$ MeV in the $^{37}\mathrm{Cl}(p, n)^{37}\mathrm{Ar}$ experiment owing to the poor energy resolution, although a slightly better energy resolution of 250 keV was achieved later [21]. In the (p, n) experiments it was also difficult to distinguish the discrete states from the continuum arising from quasifree scattering, which made it difficult to extract B(GT) values for the discrete GT states above the particle-decay threshold. Therefore, an experiment with higher resolution was desired for the study of the $^{37}\mathrm{Cl} \rightarrow {}^{37}\mathrm{Ar}$ GT transitions. In this paper we report the results of a high-energy-resolution $^{37}\mathrm{Cl}(^3\mathrm{He}, t)^{37}\mathrm{Ar}$ experiment at a beam energy of 140 MeV/nucleon and 0° scattering angle.

A high-resolution measurement of GT transitions is also interesting for the study of isospin symmetry [14]. By comparing the GT transition strengths obtained by $(^3\mathrm{He}, t)$ reactions for odd-mass nuclei with those of β decays, the $T_z = \pm 1/2$ isospin symmetry has been studied in the low-lying region of sd-shell nuclei [10,11,22]. Similarly, the isospin symmetry of GT transitions from $T_z = \pm 1$ nuclei to the 0 nucleus has been examined for a few isobars of light sd-shell nuclei, such as $A = 26$ nuclei (^{26}Mg, ^{26}Al, and ^{26}Si) [12,13] or $A = 34$ (^{34}S, ^{34}Cl, and ^{34}Ar) [23]. A good correspondence of B(GT) values with a difference of less than 5% was observed for the four strong $T_z = \pm 1 \rightarrow 0$ GT transitions in the $A = 26$ system, which suggested that the isospin symmetry was good.

The study of isospin symmetry for a system with larger T is challenging. There are several stable $T_z = +3/2$ nuclei in the sd and pf shells, for which the $T_z = +3/2 \rightarrow +1/2$ GT transitions can be studied by the use of CE reactions. On the other hand, $T_z = -3/2 \rightarrow -1/2$ transitions can be studied by using the β decays of $T_z = -3/2$ nuclei. They have relatively large Q_{EC} values exceeding 10 MeV, which allows one to study not only the transitions to the low-lying states but also the main part of the GT transition strength at higher excitation energies. Fujita *et al.* [24] extracted B(GT) values up to $E_x = 10.4$ MeV in ^{41}Ca using the $^{41}\mathrm{K}(^3\mathrm{He}, t)^{41}\mathrm{Ca}$ experiment and compared them to the B(GT) distribution obtained in the β decay of ^{41}Ti [25] to study the symmetry of the $T = 3/2$ system for $A = 41$ isobars. It was found that the overall B(GT) distributions of the two measurements were similar to each other up to 8 MeV. In addition, a correspondence of GT transitions was identified up to about 6 MeV. However, the strengths of corresponding GT transitions were not necessarily identical even when the transitions had relatively large B(GT) values of > 0.1. From the strength difference of $T_z = \pm 3/2 \rightarrow \pm 1/2$ transitions, they deduced isospin-asymmetry matrix elements of $\approx$8 keV. At the higher energy region of 6 to 8 MeV, B(GT) strengths were small and the one-to-one correspondence was not clear.

It should be noted that the $A = 37$, $T = 3/2$ system is suitable for the study of isospin symmetry at high excitation energies, because the $^{37}\mathrm{Ca} \rightarrow {}^{37}\mathrm{K}$ ($T_z = -3/2 \rightarrow -1/2$) β decay has a large Q_{EC} value of 11.6 MeV. In order to study the $^{37}\mathrm{Cl} \rightarrow {}^{37}\mathrm{Ar}$ ($T_z = 3/2 \rightarrow 1/2$) GT transitions, we have performed a high-resolution $^{37}\mathrm{Cl}(^3\mathrm{He}, t)^{37}\mathrm{Ar}$ experiment at 0° using a 140 MeV/nucleon ^{3}He beam. The B(GT) values of $T_z = 3/2 \rightarrow 1/2$ GT transitions obtained in the $^{37}\mathrm{Cl}(^3\mathrm{He}, t)^{37}\mathrm{Ar}$ experiment were compared with the $^{37}\mathrm{Ca} \rightarrow {}^{37}\mathrm{K}$ β-decay data [20]. The isospin symmetry has been examined up to $E_x = 8.6$ MeV in ^{37}Ar and in ^{37}K. By using the obtained B(GT) values, the neutrino absorption cross sections for the solar-neutrino spectra of ^{8}B were also calculated.

II. EXPERIMENT

The $^{37}\mathrm{Cl}(^3\mathrm{He}, t)^{37}\mathrm{Ar}$ experiment was performed at the Research Center for Nuclear Physics (RCNP), Osaka University,

by using the QQDD-type high-resolution magnetic spectrometer "Grand Raiden" [26] placed at 0°. A 140 MeV/nucleon ^{3}He beam from the $K = 400$ ring cyclotron [27] bombarded the ^{37}Cl compound target and was stopped by a Faraday cup inside the first dipole magnet (D1-FC) of Grand Raiden. We found that the charge detection efficiency of the D1-FC was lower by 20% compared to that of the standard Faraday cup placed at the scattering chamber, During the experiment, we used D1-FC as a beam monitor and corrected for the efficiency loss. The outgoing tritons were momentum analyzed within the full acceptance of ±17 and ±38 mr in horizontal (x) and vertical (y) directions, respectively. They were detected with a position-sensitive multiwire drift-chamber system allowing for track reconstruction [28]. The ray-trace information enabled us to subdivide the acceptance of the spectrometer by software cuts.

The difference of the energy depositions between ^{3}He and tritons in the target causes a large energy spread of the outgoing tritons. In addition, the source point should be centered at the target position of Grand Raiden to achieve a good resolution. Therefore, it is important to use a thin self-supporting target. However, pure chlorine is usually gaseous. To overcome this difficulty, we used a newly developed chlorine target made of enriched calcium chloride ($^{40}Ca^{37}Cl_2$) supported by polyvinylalcohol (PVA) [29]. The PVA consists of natural hydrogen, carbon, and oxygen. The isotopic enrichments of ^{37}Cl and ^{40}Ca were 99.8% and 99.99%, respectively. Although a large amount of ^{12}C, ^{16}O, and ^{40}Ca are included in the target, the large negative Q values of these isotopes allow us to measure the ^{37}Ar spectrum up to $E_x \sim 14$ MeV.

An energy resolution better than the energy spread of the beam was realized by applying the *dispersion matching* technique [30]. By using the beam course "WS" [31] for the beam transport and the "faint beam method" to diagnose the matching conditions [32,33], an energy resolution of 30 keV [full width at half maximum (FWHM)] was achieved. The obtained spectrum of ^{37}Cl(^{3}He, t)^{37}Ar at 0° is shown in Fig. 2.

Since our target foil contained a large amount of PVA, several peaks originating from ^{13}C and ^{18}O coexisted with the states of ^{37}Ar in the obtained spectra. In the $E_x \leqslant 6$ MeV region, most of those peaks were separated owing to the high resolution and identified by using a pure PVA spectrum taken under the same condition. We also confirmed that there was no peak of ^{35}Ar by examining the spectrum for the $^{40}Ca^{35}Cl_2$+PVA target. The 1.411- and 4.799-MeV states are assigned as GT states in Ref. [34]. However, these states completely overlapped with the g.s. and the 3.50-MeV state in ^{13}N, respectively. In the $E_x > 6$ MeV region, several small ^{13}N peaks were overlapped. Owing to the high level density of the ^{37}Ar states, it was hard to distinguish those peaks. In the analysis all strengths expected from the contaminations were subtracted.

In order to determine accurately the scattering angle Θ around 0°, angle measurements in both the x direction (θ) and y direction (ϕ) are equally important, where $\Theta \approx \sqrt{\theta^2 + \phi^2}$. Good θ resolution was achieved with the *angular dispersion matching* technique [30]. However, it is not easy to achieve a good ϕ resolution owing to the small vertical angle magnification of Grand Raiden (≈0.17). In order to improve the resolution in ϕ, we applied the "over focus mode" [35] for the spectrometer, in which the vertical position at the focal plane is proportional to the vertical angle at the target. As a result, we achieved an angular resolution of 4.5 mr for Θ.

In order to determine the scattering angle, a calibration measurement was performed using a multihole slit installed 605.5 mm downstream from the target. On the bases of this calibration of the angle, the spectra with scattering angle cuts of $\Theta = 0°$–$0.5°$, $0.5°$–$1.0°$, $1.0°$–$1.5°$, and $1.5°$–$2.0°$ were obtained. All those transitions that exhibit a relative decrease in strength were considered candidates for GT states.

The excitation energies of ^{37}Ar were determined by the use of the well-known excitation energies of ^{13}N, ^{16}F, ^{18}F, ^{24}Al, ^{26}Al, ^{35}Ar, and ^{37}Ar. They were measured under the same conditions as the targets of MgO, $^{40}Ca^{35}Cl_2$ + PVA, and $^{40}Ca^{37}Cl_2$ + PVA. By using the position measurements in the dispersive direction, x_{fp}, of the well-known states and kinematic calculations, the relationship between x_{fp} and $B\rho$ was extracted. Finally, the excitation energies of ^{37}Ar were determined from x_{fp}. The E_x values of all ^{37}Ar states were determined by interpolation. It is estimated that the systematic uncertainty of the excitation energy arising from the interpolation was 4 keV. Some states have additional uncertainties due to the ambiguity of the peak decomposition, which is explained in Sec. III.

III. ANALYSIS

The ^{37}Cl(^{3}He, t)^{37}Ar spectrum at 0° is shown in Fig. 2. We see many discrete states especially in the region above 7 MeV

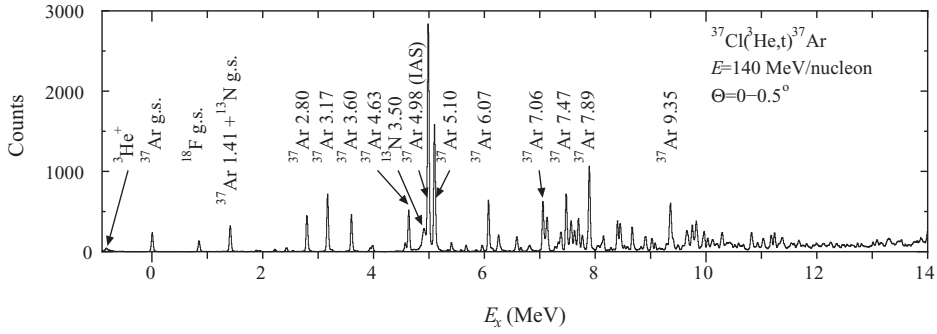

FIG. 2. Energy spectrum of the ^{37}Cl(^{3}He, t)^{37}Ar experiment at $\Theta = 0°$–$0.5°$. The energy resolution is 30 keV (FWHM).

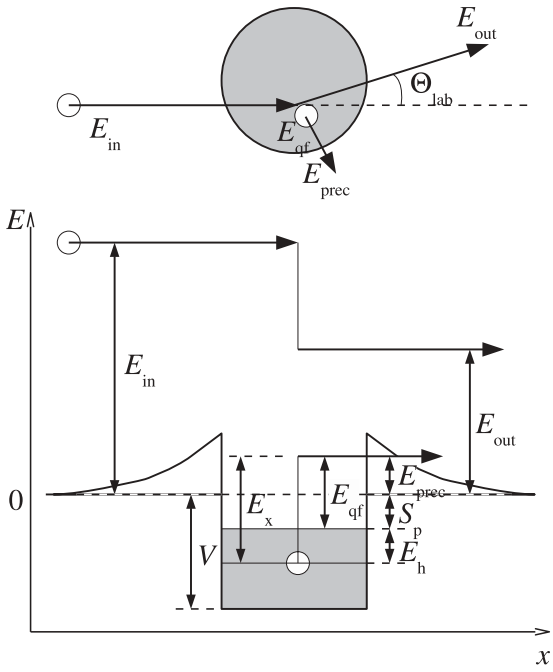

FIG. 3. Schematic description of quasifree scattering. The upper drawing shows the the trajectories and the lower drawing the energies. The drawings are not to scale.

owing to the high resolution achieved in our measurements. In addition, the strength of the underlying continuum looks much smaller than in the (p, n) spectrum [8]. We see that the strengths of the structured discrete states are well distinguished from the smooth continuum. The procedure of separating the discrete states and the continuum is described in the following sections.

A. Separation of the discrete states and the continuum

The reaction in which the incident particle directly knocks out a nucleon in the target nucleus is called "quasifree scattering." A schematic description of the quasifree scattering is given in Fig. 3. Due to the three-body nature of the reaction, it produces a continuum above the proton separation energy of $S_p = 8.715$ MeV in the triton spectrum. Since we measured only the singles spectrum, it is impossible to estimate the contribution of the quasifree scattering caused by the ^{37}Cl(^{3}He, tp)^{36}Cl reaction. The $\sigma\tau$ operator in the effective ^{3}He-nucleon interaction can also cause the quasifree scattering. In this paper, however, we focus on the discrete states, for which the assignment of the angular-momentum transfer ($\Delta L = 0$) can be deduced from the measured angular distribution. Therefore, the quasifree scattering should be subtracted as background.

In order to estimate the contribution of quasifree scattering to the continuum, a phenomenological function was used [36,37]. The function was based on the classical scattering between the incident particle and a nucleon inside the target nucleus. Although this function could reproduce the experimental continuum at very high excitation energies of more than 20 MeV, we found that it was not accurate enough to reproduce the shape of the continuum just above the particle separation energy. Therefore, we derived an improved phenomenological function by taking the penetrability of the emitted proton into account:

$$\frac{d^2\sigma_{\rm qf}}{d\Omega dE}(E_x) = N_0 P(E_x)\frac{1-\exp\left(-\frac{E_x-S_{\rm p}-E_{\rm h}}{T}\right)}{1+\left(\frac{E_x-E_{\rm qf}}{W}\right)^2} \quad (\text{if } E_{\rm x} > S_{\rm p}), \tag{1}$$

where E_x, S_p, and $E_{\rm h}$ are the excitation energy, the proton separation energy, and the energy depth of the hole state from the Fermi surface in the daughter nucleus. The numerator represents the effect of the Pauli blocking, in which the parameter T has the dimension of energy and shows the diffusion of the Fermi surface. Since the continuum at lower excitation energies is dominantly produced by the emission of a proton bound on the Fermi surface, we assumed $E_h = 0$ MeV. The denominator, which makes a broad bump with a width of $2W$ and a peak at $E_{\rm qf}$, shows the effect of the Fermi motion of the nucleon inside the nucleus. $P(E_x)$ represents the penetrability of the recoil proton through the Coulomb and the centrifugal potential barriers that are hindering the emission of the recoil proton. N_0 is a normalization factor.

If the Fermi motion is ignored, the excitation energy of the quasifree scattering is concentrated at $E_{\rm qf}$, which is equal to the recoil-proton energy of the n(^{3}He, t)p reaction. In reality, the Fermi motion gives the recoil energy a width of $2W$ centered around $E_{\rm qf}$. In order to reproduce the continuum around 0° a $E_{\rm qf}$ value of more than 10 MeV was used in previous studies [36,37] to take into account the effect of the binding energy and the Coulomb barrier for the recoil proton. However, we should note that $E_{\rm qf}$ is not affected by either the binding energy or the Coulomb barrier. It is determined only by kinematics. The binding energy should be involved in the numerator related to the Pauli blocking. Such an $E_{\rm qf}$ value exceeding 10 MeV is possible only if a singles spectrum is measured at large backward angles. The $E_{\rm qf}$ value at forward angles should be very small. We found that, if the energy resolution of the spectrum is poor, the large $E_{\rm qf}$ value looks reasonable even at very forward angles. When a triton is emitted at 0.3°, corresponding to an average scattering angle of the range of 0° to 0.5°, the recoil-proton energy $E_{\rm qf}$ is 0.06 MeV.

If the recoil proton is excited just above the proton separation energy, the Coulomb and the centrifugal potential barriers hinder the emission of the recoil proton. In $P(E_x)$ of Eq. (1) the Coulomb potential is proportional to $1/r$, where r is the radius of a nucleus. The centrifugal potential is proportional to $1/r^2$. The knockout protons mainly populate the d orbit, with an angular momentum $L = 2$. Since the strengths of the centrifugal and the Coulomb potentials are similar, we folded the effect of the centrifugal potential into the Coulomb barrier by adjusting the parameters. By using the WKB approximation P is expressed as

$$P(E_x) = \exp\left[-\frac{2\sqrt{2}BR}{\hbar}\sqrt{\frac{M}{E_x-S_p}}(\cos^{-1}\theta_0 - \sqrt{\cos\theta_0(1-\cos\theta_0)})\right], \tag{2}$$

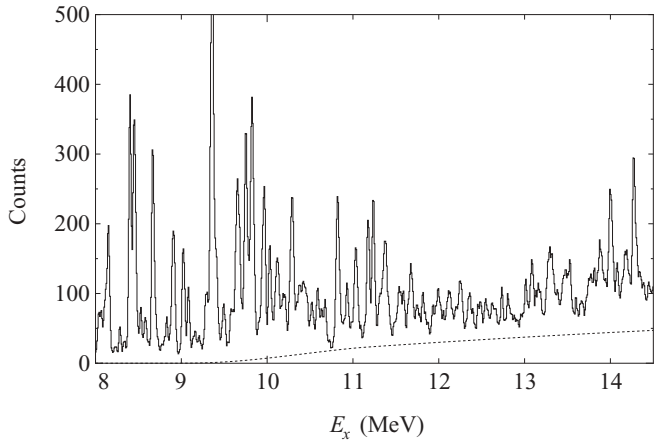

FIG. 4. A part of the energy spectrum. The counts indicated by the dotted line were calculated with Eq. (1). They were subtracted as quasifree scattering events in the analysis.

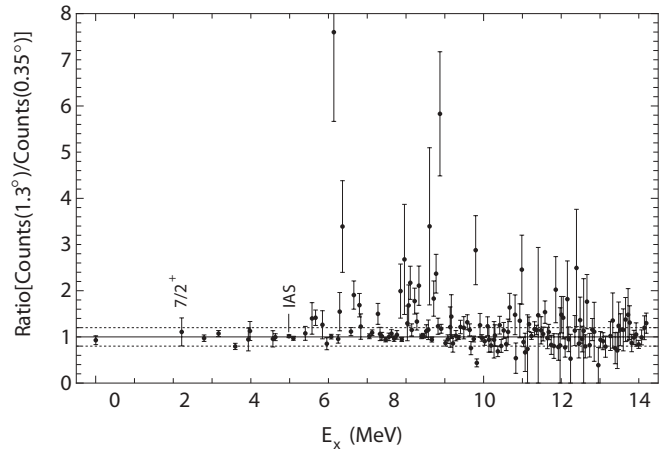

FIG. 5. Ratios of counts for scattering angles $\Theta = 1.0^\circ$–1.5° and $\Theta = 0.0^\circ$–0.5°. The dotted lines show the 20% differences from unity. Transitions with the error bars overlapping the region between two dotted lines were identified as $\Delta L = 0$.

where

$$\cos\theta_0 = \sqrt{E_{\rm prec}/B}. \tag{3}$$

Here $E_{\rm prec} = E_x - S_{\rm p} - E_{\rm h}$ is the energy of the recoil proton. B is the magnitude of the Coulomb potential at the nuclear surface defined by

$$B = \frac{C_0}{4\pi\varepsilon}\frac{Zze^2}{R}, \tag{4}$$

where C_0 is a constant to adjust the magnitudes of the potential barrier. Z and z are proton numbers of the residual nucleus and the knocked-out proton, i.e., $z = 1$. The nuclear radius, R, was determined by $R = 1.1A^{1/3}$ fm. The values of N_0 in Eq. (1) and C_0 in Eq. (4) were adjusted in the process of the peak decomposition of the spectrum.

A peak-decomposition program was used to separate each of the discrete states and the continuum. The well-separated peak at 2.80 MeV was used as a standard for the peak shape. N_0 and C_0 in Eq. (1) and Eq. (4) were determined to minimize the χ^2 value in the process of peak decomposition. After several trials by changing the parameters N_0 and C_0, it was estimated that the uncertainty of the intensity of the continuum was about 20%. Figure 4 shows the deduced continuum noticeable at higher excitation energies. The final values of the parameters in Eq. (1) and (4) are summarized in Table I.

In order to identify $\Delta L = 0$ transitions, we compared the counts in the angle ranges $\Theta = 0^\circ$–0.5° and $\Theta = 1.0^\circ$–1.5° for each peak. Figure 5 shows the ratio of the intensities for each peak between $\Theta = 0^\circ$–0.5° and $\Theta = 1.0^\circ$–1.5°, where the ratios are normalized so that the average value of the ratio for the strong 13 transitions in the excitation energy region $E_x = 5.93$–8.15 MeV is unity. We found that the ratios for the states at 0, 2.50, 3.17, 3.60, 3.94, and 4.63 MeV, known to be $\Delta J = 1^+$ GT states [34], were unity within 20% uncertainty. For other states we selected transitions as $\Delta L = 0$ if the error bars of the ratios overlapped with the ratios from 0.8 to 1.2. All prominent peaks had ratios within this range.

For weakly excited states, the identification of $\Delta L = 0$ is uncertain. For example, the ratio is 1.1 for the state at 2.22 MeV, with spin-parity $J^\pi = 7/2^+$. This indicates that some of the $\Delta L = 2$ transitions have angular distributions similar to $\Delta L = 0$ transitions near 0°. However, the differential cross section of the $L = 2$ transition in the 0°–0.5° spectrum was very small with a corresponding $B(\mathrm{GT}) < 0.01$. Another possibility of misidentification results from the incompleteness of the peak decomposition. Some $\Delta L = 0$ states influenced by $\Delta L \leqslant 1$ transitions could be rejected, while small $\Delta L \leqslant 1$ transitions buried in $\Delta L \leqslant 1$ transitions could be accepted. A few states showed ratios of less than 0.8. They can be produced by the ambiguity of the continuum subtraction and the peak fitting.

B. Extraction of GT strength

It is known that, in CE reactions, the cross sections for GT transitions are approximately proportional to $B(\mathrm{GT})$ values in the limit of the momentum transfer $q = 0$ [9–13]:

$$\frac{d\sigma}{d\Omega}(q=0) = K N_{\sigma\tau} |J_{\sigma\tau}|^2 B(GT) \tag{5}$$

$$= \hat{\sigma}_{\rm GT} B(\mathrm{GT}), \tag{6}$$

where $J_{\sigma\tau}$ is the volume integral of the effective interaction $V_{\sigma\tau}$ at momentum transfer $q = 0$, K is the kinematic factor, $N_{\sigma\tau}$ is a distortion factor, and $\hat{\sigma}_{\rm GT}$ is the unit cross section for the GT transition. At finite momentum transfer q or finite energy loss $\omega = Q + E_x$, the differential cross section becomes [9,14]

$$\frac{d\sigma}{d\Omega}(q,\omega) = \hat{\sigma} F(q,\omega) B(\mathrm{GT}), \tag{7}$$

where $F(q,\omega)$ becomes unity in the limit of $q = 0$ and $\omega = 0$. For small q and ω, $F(q,\omega)$ is almost independent of the wave functions of the final states. In our experiment, we do not know the absolute differential cross section because we did not determine the target thickness accurately. However, we know the accurate counts $N_{\rm GT}(q,\omega)$ in the spectrum. Therefore, we can extract the proportionality between $N_{\rm GT}(q,\omega)$ and $B(\mathrm{GT})$,

$$N_{\rm GT}(q,\omega) = \hat{N}_{\rm GT} F(q,\omega) B(\mathrm{GT}), \tag{8}$$

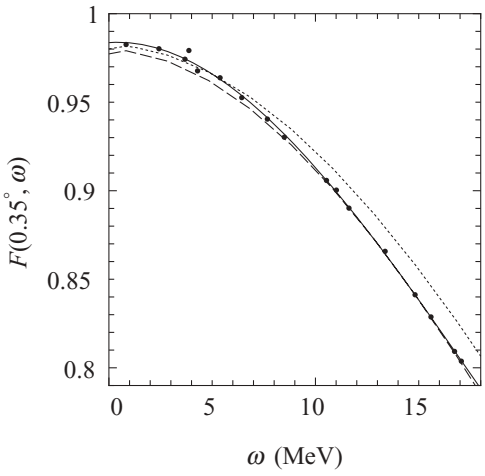

FIG. 6. Correction function $F(\theta_{\rm lab} = 0.35^\circ, \omega)$ obtained by using DWBA calculations. The filled circles show the DWBA calculations using the shell-model wave functions for individual states. The solid curve fits these filled circles with a quadratic function. The dotted and dashed curves show the DWBA calculations with pure $(d_{3/2}, d_{3/2}^{-1})$ and $(d_{3/2}, d_{5/2}^{-1})$ configurations, respectively, assumed. For $E_x < 5$ MeV, the filled circles are distributed along the dotted line. Above $E_x = 5$ MeV, the filled circles follow the dashed line.

where $\hat{N}_{\rm GT}$ is the unit count defined by the ratio of $N_{\rm GT}(q = 0, \omega = 0)$ and B(GT).

The excitation-energy dependence of $F(q, \omega)$ for the ^{37}Cl(^{3}He, t)^{37}Ar reaction was calculated by using the distorted-wave Born approximation (DWBA) code DW81, where $\Theta_{\rm lab}$ was fixed at 0.35°, the average of the angular acceptance of the 0°–0.5° spectrum. The filled circles in Fig. 6 indicate the $F(q, \omega)$ factors for prominent GT states. The one-body transition densities were obtained using the shell-model (SM) code OXBASH [38] where the universal sd-shell (USD) interaction [39] was used. The solid line shows the quadratic fit to the filled circles, which were used to extract the B(GT) values using Eq. (9). The dotted and the dashed lines indicate the cross sections with a pure $d_{3/2} \rightarrow d_{3/2}$ and a pure $d_{5/2} \rightarrow d_{3/2}$ transition, respectively, assumed. The filled circles are distributed along the $d_{3/2} \rightarrow d_{3/2}$ line at lower excitation energies. On the other hand, the filled circles follow the $d_{3/2} \rightarrow d_{5/2}$ line as the excitation energy increases. This change suggests that the dominant one-body transition density changes from $d_{3/2} \rightarrow d_{3/2}$ to $d_{5/2} \rightarrow d_{3/2}$ transitions.

In order to extract the B(GT) values by using Eq. (9), we need a standard B(GT) value. One option is to use the empirical B(GT) value obtained by the β decay of the $J^\pi = 3/2^+$ g.s. of ^{37}Ar feeding the $J^\pi = 3/2^+$ g.s. of ^{37}Cl. This transition strength is exactly the same as the transition of ^{37}Cl(g.s.) $\rightarrow$ ^{37}Ar(g.s.), although the direction is reversed. [Since the spin relationships of the ^{37}Cl(g.s.) $\rightarrow$ ^{37}Ar(g.s.) and the ^{37}Ar(g.s.) $\rightarrow$ ^{37}Cl(g.s.) transitions are equal, no conversion factor for the spin geometry is needed.] However, the SM calculation suggests that this transition has mainly the configuration of $(d_{3/2}, d_{3/2}^{-1})$, and there are several reports showing that the proportionality between the cross sections and the B(GT) values is not necessarily well kept in the $(j_< \rightarrow j_<)$-type transitions [40–42]. In addition, this transition is rather weak [$B(GT) = 0.036$]. It is known that the proportionality is less reliable for weak transitions [13,14,23]. Therefore, we concluded that the ^{37}Cl(g.s.) $\rightarrow$ ^{37}Ar(g.s.) transition is not suitable for use as a normalization standard. The better option is to use the B(GT) values from the isospin-symmetrical ^{37}Ca β decay. Due to the large $Q_{\rm EC}$ value of ^{37}Ca β decay, many GT transitions have been observed up to $E_x = 8.6$ MeV in ^{37}K [19,20]. The sum of their strengths is large enough to be used for the normalization. In selecting the region of excitation energy to be used for the normalization, we considered the following: (1) The proportionality between the cross sections and the B(GT) values in the ^{37}Cl(^{3}He, t)^{37}Ar reaction can have an ambiguity larger than 20% at lower excitation energies, namely, $E_x < 5$ MeV. (2) The errors of the β-decay data are large in the highly excited energy region of $E_x > 8.5$ MeV, because the branching ratio of the β decay rapidly decreases as the excitation energy increases. (3) There are many GT states having moderate strengths in the excitation-energy region between 5.93 and 8.15 MeV. Therefore, we only used the B(GT) values in the region between $E_x = 5.93$ and 8.15 MeV for the normalization. The total B(GT) value of ^{37}Ca β decay in this energy region was 0.942 ± 0.019.

TABLE I. Parameter set of Eqs. (1), (2), and (4).

T	100 MeV
$S_{\rm p}$	8.7151 MeV
$E_{\rm h}$	0.0 MeV
W	22 MeV
$E_{\rm qf}$	0.06 MeV
C_0	0.3
N_0	1200

The deduced B(GT) values are listed in Tables II, III, and IV, and compared to the ^{37}Ca β decay B(GT) values [20]. Note that the isobaric analogue state (IAS) contains the strength of both GT and Fermi transitions. As in the case of the GT transition, the Fermi transition also has a proportionality, i.e.,

$$N_{\rm F} = \hat{N}_{\rm F} F(q, \omega) B({\rm F}), \tag{9}$$

where $N_{\rm F}$, $\hat{N}_{\rm F}$, and B(F) are the counts, the unit count, and the strength of the Fermi transition. In order to extract the GT strength in IAS [$B(\rm GT)_{\rm IAS}$], we subtracted the strength arising from the Fermi transition using the following relationship:

$$\begin{aligned} B({\rm GT})_{\rm IAS} &= \frac{1}{\hat{N}_{\rm GT}}(N_{\rm IAS} - N_{\rm F}) \\ &= \frac{1}{\hat{N}_{\rm GT}}[N_{\rm IAS} - \hat{N}_{\rm F} B({\rm F})] \\ &= \frac{N_{\rm IAS}}{\hat{N}_{\rm GT}} - \frac{B({\rm F})}{R^2}, \end{aligned} \tag{10}$$

where $N_{\rm IAS}$ is the number of total counts of the IAS and $R^2 \equiv \hat{\sigma}_{\rm GT}/\hat{\sigma}_{\rm F} = \hat{N}_{\rm GT}/\hat{N}_{\rm F}$. We used $R^2 = 7.1 \pm 0.7$ [43], which was obtained from the systematics of the empirical R^2 values as a function of nuclear mass, and B(F) = 3 under the assumption that the Fermi strength is concentrated in the transition to the 4.98-MeV IAS.

TABLE II. The B(GT) values obtained from the ^{37}Cl(^{3}He, t)^{37}Ar and ^{37}Ca β-decay data [19,20]. The B(GT) values from ^{37}Ca β decay listed in Ref. [20] were divided by $(g_A/g_V)^2 = (1.262 \pm 0.004)^2$ because of a different definition of B(GT)

States in ^{37}Ar					States in ^{37}K				
Evaluated values[a]		^{37}Cl(^{3}He, t)[b]			^{37}Ca β decay[c]			^{37}Ca β decay[d]	
E_x(MeV)	$2J^\pi;2T$	E_x(MeV)	Counts	B(GT)	E_x(MeV)	$2J^\pi;2T$	B(GT)	E_x(MeV)	B(GT)
0.000(0)	3^+	0.000(0)	1142(46)	0.0348(17)	0.000(0)	3^+	0.035(4)	0.0	0.0301(13)
1.40982(10)	1^+	1.410(4)	293(95)	0.009(3)	1.3700(0)	1^+	0.0078(4)	1.3709	0.0079(4)
2.7961(3)	5^+	2.795(4)	2249(65)	0.069(3)	2.751(4)	5^+	0.062(9)	2.7504	0.064(2)
3.1713(14)	5^+	3.167(4)	3310(110)	0.102(4)	3.240(2)	5^+	0.048(12)	3.2393	0.0055(3)
3.6020(7)	3^+	3.598(4)	2110(88)	0.065(3)	3.623(2)	3^+	0.0448(13)	3.6222	0.0458(13)
3.9367(4)	3^+	3.935(5)	221(24)	0.0068(8)	3.839(3)		0.0507(15)	3.8402	0.058(2)
3.9798(8)	$(1–5^+)$	3.977(4)	364(29)	0.0113(10)	3.853(3)		0.0064(3)		
					4.192(9)		0.0018(2)		
4.5731(10)	$(3, 5^+)$	4.568(4)	458(45)	0.0143(15)	4.415(2)	$(1, 3)^+$	0.0258(8)		
4.6343(7)	3^-	4.632(4)	2414(96)	0.075(4)	4.496(3)	1^+	0.0339(11)		
4.7985(10)	$(3, 5^+)$								
					5.017(4)	3^+	0.000(14)		
4.993(6)[e]	$3^+;3$	4.983(4)[e]	13700(270)	$0.01(^{+4}_{-1})$	5.050(3)	$3^+;3$	0.06(5)		
5.1017(12)	$(3, 5^+)$	5.097(4)	7210(170)	0.226(8)	5.120(3)	1^+	0.254(8)		
					5.358(6)		0.0014(3)		
		5.152(6)	126(31)	0.0040(10)	5.424(2)		0.0059(8)		
		5.339(5)	114(16)	0.0036(5)	5.459(4)		0.0187(9)		
		5.404(4)	565(33)	0.0178(11)	5.480(2)		0.0013(3)		
		5.577(5)	102(17)	0.0032(6)	5.624(2)		0.0096(7)		
					5.713(4)		0.00043(12)		
					5.789(5)		0.0030(3)		
					5.933(4)		0.0148(8)		
		5.846(5)	109(18)	0.0035(6)	6.015(2)		0.057(2)		
		5.958(4)	360(33)	0.0114(11)	6.092(2)		0.0398(18)		
		6.072(4)	2897(90)	0.092(4)	6.274(5)		0.0009(3)		
		6.251(4)	1094(53)	0.035(2)	6.324(5)		0.0158(9)		
		6.292(6)	207(41)	0.0066(13)	6.416(5)		0.0114(9)		
		6.580(4)	1046(53)	0.034(19)	6.432(3)		0.0205(13)		
		6.833(5)	233(41)	0.0075(13)	6.606(5)		0.0042(5)		
					6.684(5)		0.0031(4)		
					6.740(5)		0.0021(4)		
					6.974(5)		0.0380(16)		
		7.055(4)	3093(93)	0.100(4)	7.071(3)		0.067(5)		
		7.126(4)	2280(81)	0.074(3)	7.183(3)		0.049(5)		
					7.240(5)		0.0133(11)		
		7.330(4)	555(48)	0.0180(16)					
		7.377(4)	1244(65)	0.040(2)	7.370(3)		0.074(5)		
		7.474(4)	3456(99)	0.113(4)	7.4738(18)		0.116(8)		
		7.559(4)	2005(77)	0.065(3)	7.542(3)		0.025(2)		
		7.625(4)	1249(63)	0.041(2)	7.634(3)		0.070(5)		
		7.693(4)	2038(79)	0.067(3)	7.662(5)		0.0155(16)		
		7.765(4)	942(55)	0.031(2)					
		7.890(4)	5170(150)	0.170(7) }	7.8065(35)		0.146(10)		
					7.8352(42)		0.107(8)		
		8.034(2)	300(58)	0.0099(19)	8.0291(51)		0.051(6)		
		8.146(3)	849(65)	0.028(3)					
		5.85–8.15[f]		0.942(19)[g]	5.93–8.03[f]		0.942(19)[h]		

[a]From Ref. [34].
[b]This work.
[c]From Ref. [20].
[d]From Ref. [19].
[e]IAS.
[f]Excitation energy region used for normalization. See text.
[g]Normalization standard to extract B(GT) values. See text.
[h]The sum of B(GT) strength assumed to exist in the region of $E_x = 5.93$–8.03. See text.

TABLE III. The same as Table II, but for the higher excited region.

^{37}Cl(^{3}He, t^{37})Ar			^{37}Ca → ^{37}K β decay[a]	
E_x (MeV)	Counts	(GT)	E_x (MeV)	B(GT)
			8.273(5)	0.018(5)
8.280(4)	223(23)	0.0074(8)	8.314(5)	0.031(5)
8.398(4)	1757(61)	0.058(3)	8.378(5)	0.008(5)
8.450(4)	1763(61)	0.059(3)	8.429(5)	0.008(5)
8.522(4)	321(29)	0.0107(10)	8.486(5)	0.016(8)
8.575(5)	280(41)	0.0093(14)	8.525(5)	0.014(6)
8.665(4)	1537(56)	0.051(2)	8.605(5)	0.013(6)
			8.653(5)	0.010(6)
0–8.653		$1.74(^{+5}_{-2})$[b]	0–8.653	1.70(3)[c]
8.825(4)	293(27)	0.0098(9)		
8.906(4)	979(65)	0.033(2)		
9.019(4)	782(39)	0.026(2)		
9.079(4)	476(32)	0.0160(12)		
9.138(7)	156(44)	0.0053(15)		
9.167(9)	146(40)	0.0049(14)		
9.208(6)	177(24)	0.0060(9)		
9.286(4)	572(46)	0.0194(17)		
9.352(4)	3460(110)	0.117(5)		
9.404(5)	703(64)	0.024(2)		
9.489(4)	445(40)	0.0152(14)		
9.579(5)	434(41)	0.0148(15)		
9.640(4)	1200(110)	0.041(4)		
9.673(5)	790(110)	0.027(4)		
9.746(4)	1749(88)	0.060(3)		
9.824(4)	1830(160)	0.063(6)		
9.908(6)	265(40)	0.0091(18)		
9.956(4)	1371(70)	0.047(3)		
10.028(4)	804(53)	0.0296(85)		
10.103(5)	643(90)	0.022(3)		
10.141(6)	365(85)	0.013(3)		
10.194(5)	467(43)	0.0162(17)		
10.263(6)	476(170)	0.017(6)		
10.292(4)	893(173)	0.031(6)		
10.362(5)	475(47)	0.0166(19)		
10.410(5)	460(53)	0.016(2)		
10.453(5)	461(52)	0.016(2)		
10.517(5)	396(39)	0.0139(16)		
10.583(5)	479(46)	0.0168(19)		
10.631(6)	263(44)	0.0092(18)		
10.812(6)	845(230)	0.030(8)		
10.832(12)	461(230)	0.016(8)		
10.928(4)	353(37)	0.0125(19)		
11.028(4)	794(49)	0.028(2)		
11.070(8)	122(30)	0.0043(15)		
11.132(8)	93(28)	0.0033(15)		
11.172(4)	720(58)	0.026(4)		
11.233(4)	1041(49)	0.037(2)		
11.313(4)	427(34)	0.0154(18)		
11.365(4)	861(50)	0.031(2)		
11.407(5)	234(41)	0.008(2)		
11.482(5)	195(24)	0.0070(15)		
11.534(4)	459(37)	0.0166(19)		
11.645(5)	315(46)	0.012(2)		
11.680(5)	524(51)	0.019(2)		
11.745(4)	277(34)	0.010(2)		
11.810(4)	337(37)	0.012(2)		
11.926(5)	250(31)	0.0092(18)		
11.971(7)	166(50)	0.006(3)		

[a]From Ref. [20].
[b]Integrated B(GT) value up to $E_x = 8.653$ MeV.
[c]Total B(GT) value obtained in the ^{37}Ca → ^{37}K β-decay study up to $E_x = 8.653$ MeV [20].

TABLE IV. The B(GT) values obtained from the ^{37}Cl(^{3}He, t)^{37}Cl measurement in the region above $E_x = 12$ MeV.

^{37}Cl(^{3}He, t)^{37}Ar		
E_x(MeV)	Counts	B(GT)
12.003(7)	292(54)	0.011(3)
12.051(6)	174(28)	0.0064(18)
12.101(5)	333(41)	0.012(2)
12.159(6)	124(26)	0.005(3)
12.241(5)	289(33)	0.011(2)
12.345(5)	302(57)	0.011(3)
12.455(6)	222(46)	0.008(2)
12.489(7)	200(44)	0.008(2)
12.541(5)	279(40)	0.011(2)
12.579(11)	67(32)	0.003(3)
12.621(6)	257(34)	0.010(2)
12.665(6)	181(30)	0.007(2)
12.731(4)	242(30)	0.009(2)
12.802(5)	318(30)	0.012(2)
12.851(6)	111(26)	0.004(2)
12.957(6)	112(32)	0.004(3)
13.012(5)	437(41)	0.017(3)
13.079(4)	590(55)	0.023(3)
13.142(6)	396(45)	0.015(3)
13.266(5)	330(45)	0.013(3)
13.314(5)	197(39)	0.008(3)
13.375(5)	211(40)	0.008(3)
13.437(6)	370(120)	0.014(5)
13.477(7)	350(100)	0.014(5)
13.523(5)	410(80)	0.016(5)
13.596(5)	196(37)	0.008(3)
13.658(5)	221(39)	0.009(3)
13.723(6)	287(70)	0.011(4)
13.766(6)	415(72)	0.017(4)
13.816(6)	477(52)	0.019(3)
13.875(5)	749(69)	0.030(4)
13.932(5)	409(55)	0.016(3)
13.997(4)	1327(82)	0.053(4)
14.072(5)	555(45)	0.022(3)
14.143(5)	488(65)	0.020(4)
14.192(5)	642(69)	0.026(4)
0–14.20		$3.34(^{+6}_{-3})$[a]

[a]Total B(GT) strength obtained by this study in the energy region up to 14.20 MeV.

The uncertainties of the obtained B(GT) except of the IAS come only from the ambiguities of the peak fitting and the total B(GT) value of ^{37}Ca β decay used in the normalization. The ambiguity of the proportionality is not included. The uncertainty of the B(GT) value for the IAS contains an additional ambiguity of the R^2 value. Therefore, the uncertainty of the B(GT) value for the IAS is relatively large.

IV. DISCUSSION

A. Comparison with ^{37}Ca β decay

As shown in Table II, we found 11 pairs of corresponding GT states at excitation energies E_x below 5.1 MeV in ^{37}Ar and ^{37}K, namely, at 0.0, 1.41, 2.80, 3.17, 3.60, 3.94, 3.98, 4.57, 4.63, 4.98, and 5.10 MeV in ^{37}Ar. The consistency of the J^π values for the five pairs at $E_x < 3.6$ MeV suggests that they are isobaric analog states. The two doublets at 3.94 and 3.98 MeV and at 4.57 and 4.63 MeV in ^{37}Ar have similar excitation energies to the doublets at 3.84 and 3.85 MeV and at 4.41 and 4.50 MeV in ^{37}K. Although the J^π values of these states are uncertain except for the 3.94-MeV state in ^{37}Ar, the excitation energies are similar. This suggests that the pairs of states at 3.94 and 3.98 MeV and at 4.57 and 4.63 MeV in ^{37}Ar are isobaric analog to the pairs at 3.84 and 3.85 MeV and at 4.41 and 4.50 MeV in ^{37}K, respectively. The energy differences of corresponding states in ^{37}Ar and ^{37}K are at most 150 keV. The good correspondences indicate that the isospin symmetry in terms of the excitation energy is rather good.

No state corresponding to the 4.19-MeV state in ^{37}K was observed in ^{37}Ar using the ^{37}Cl(^{3}He, t)^{37}Ar reaction. The excitation energies are similar for the 5.10-MeV state in ^{37}Ar and the 5.12-MeV state in ^{37}K and the B(GT) values are consistent. This suggests that these states are isobaric analog states. However, the assigned J^π values for the 5.10-MeV state in ^{37}Ar [34] and the 5.12-MeV state in ^{37}K [20] are inconsistent. We could not find a state corresponding to the 5.02-MeV state in ^{37}K in the ^{37}Cl(^{3}He, t)^{37}Ar spectrum. Unfortunately, the 3.50-MeV state in ^{13}N originated from the ^{13}C contaminant (see Fig. 2).

In Fig. 7 the B(GT) distributions for the ^{37}Cl $\rightarrow$ ^{37}Ar transitions are compared with those of the ^{37}Ca $\rightarrow$ ^{37}K transitions. Clusters with similar strengths exist at similar excitation energies, i.e., 2.5–4.0, 4.0–5.5, 5.7–6.7, 6.7–8.0, and 8.2–8.7 MeV. This shows that the overall isospin symmetry is rather good. In Fig. 8 the cumulative sums of the B(GT) values as a function of excitation energy are compared to the ^{37}Cl $\rightarrow$ ^{37}Ar and ^{37}Ca $\rightarrow$ ^{37}K transitions. The two curves are very similar. This also suggests good isospin symmetry.

Although the overall symmetry of ^{37}Cl $\rightarrow$ ^{37}Ar and ^{37}Ca $\rightarrow$ ^{37}K GT transitions is good, B(GT) values for individual corresponding states, deduced from the ^{37}Cl(^{3}He, t)^{37}Ar and ^{37}Ca β-decay measurements, are not necessarily in agreement. For instance, the B(GT) values of the 3.17-MeV state in ^{37}Ar and the 3.24-MeV state in ^{37}K are different by a factor of 2. The sum of the B(GT) values of the 3.94- and 3.98-MeV states in ^{37}Ar is different from the corresponding doublets in ^{37}K by a factor of 3. Such a difference is also seen for the 4.57–4.63 MeV doublet in ^{37}Ar and the 4.41–4.50 MeV doublet in ^{37}K.

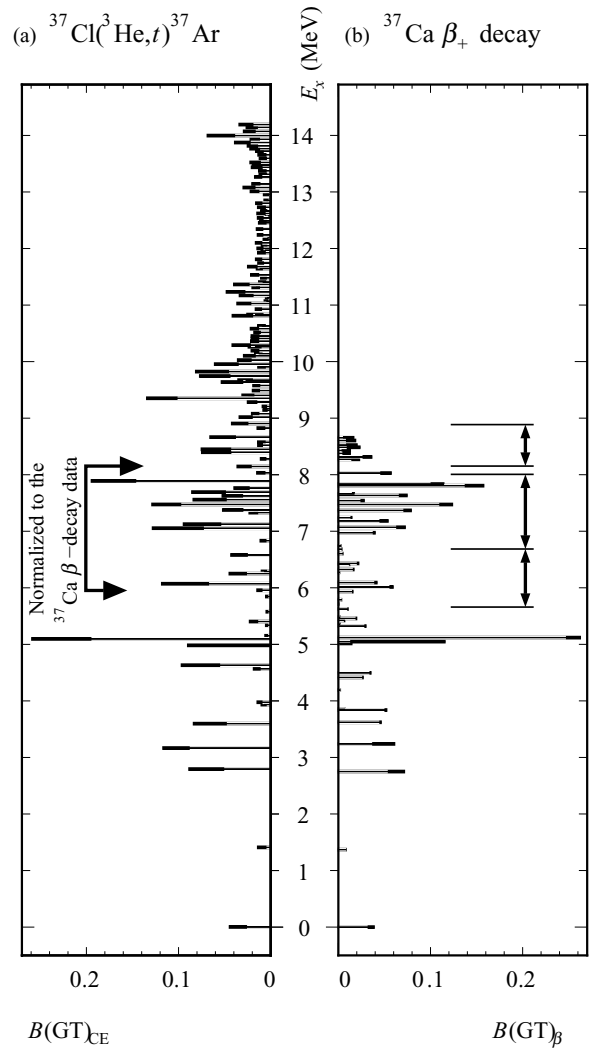

FIG. 7. Comparison of experimental B(GT) distributions of ^{37}Cl $\rightarrow$ ^{37}Ar and ^{37}Ca $\rightarrow$ ^{37}K GT transitions obtained from ^{37}Cl(^{3}He, t)^{37}Ar and ^{37}Ca β decay [20] measurements, respectively. The ^{37}Cl $\rightarrow$ ^{37}Ar B(GT) values are normalized by using the ^{37}Ca β-decay data [20] in the region $E_x = 5.93$–8.15 MeV. The thin and thick bars indicate the B(GT) values and uncertainties, respectively. The regions of the clusters having similar strengths between the ^{37}Cl $\rightarrow$ ^{37}Ar and ^{37}Ca $\rightarrow$ ^{37}K GT transitions are indicated by the arrows. These regions in 5.7–6.7, 6.7–8.0, and 8.2–8.7 MeV are indicated in (b).

At higher excitation energies, three clusters with similar strengths are seen in the energy regions of 5.7–6.7, 6.7–8.0, and 8.2–8.7 MeV in both ^{37}Cl $\rightarrow$ ^{37}Ar and ^{37}Ca $\rightarrow$ ^{37}K transitions, as shown in Fig. 7. Also here, the strengths for the individual states are not necessarily in agreement and some levels have no corresponding pair in the mirror nucleus. A similar finding is reported for the $T_z = \pm 3/2 \rightarrow \pm 1/2$ GT transitions in the $A = 41$ system [24].

There are two possible explanations for the differences seen in the $E_x < 5.1$ MeV region and in the $E_x > 5.1$ MeV region. One possibility is an isospin asymmetry between

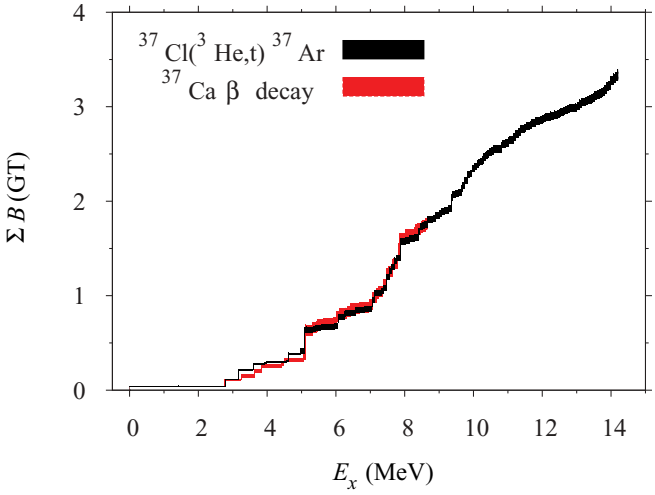

FIG. 8. (Color online) Comparison of cumulative sums of B(GT) between ^{37}Cl → ^{37}Ar (gray, red online) and ^{37}Ca → ^{37}K (black) GT transitions by ^{37}Cl(^{3}He, t)^{37}Ar and ^{37}Ca β decay [20], respectively. The band widths represent the accumulated errors.

the ^{37}Cl → ^{37}Ar and ^{37}Ca → ^{37}K transitions. High level densities at highly excited energies may lead to different strengths for mirror transitions by configuration mixing. Another possibility is the anomaly of the proportionality between the 0° differential cross sections and the B(GT) values in the ^{37}Cl(^{3}He, t)^{37}Cl reaction. There are reports that the ambiguity of the proportionality in the case of the $j_< \rightarrow j_<$ transition becomes large [40–42].

If one assumes that the nuclear interaction is charge independent, the nuclear structures of mirror nuclei are identical. In real nuclei, however, the Coulomb force, which breaks isospin symmetry, is not negligibly small. Therefore, some deviations from the symmetrical structure are expected. In order to estimate the effect of the Coulomb force causing asymmetry between the ^{37}Cl → ^{37}Ar and ^{37}Ca → ^{37}K transitions, a SM calculation was performed by using the code OXBASH with the isospin-nonconserving USD interaction (USD-INC). The effect of the limited model space was compensated for by introducing a quenching factor for the B(GT) values [19,44,45],

$$B(\mathrm{GT})_{\mathrm{eff}} \approx [1 - 0.248(A/28)^{0.35}]^2 B(\mathrm{GT})_{\mathrm{free}}, \qquad (11)$$

where A is the nuclear mass. For $A = 37$, the quenching factor is 0.53.

The calculated B(GT) distributions for the ^{37}Cl → ^{37}Ar and ^{37}Ca → ^{37}K transitions are shown in Fig. 9. Although the SM calculation could not reproduce the number of fragmented GT states observed in the ^{37}Cl(^{3}He, t)^{37}Al measurement, it is still useful to study the basic nature of isospin symmetry and its breaking by the Coulomb force. Figure 9 shows that the gross features of the B(GT) distributions are similar for the ^{37}Cl → ^{37}Ar and ^{37}Ca → ^{37}K transitions. As shown in Fig. 10, the cumulative sums of these B(GT) values as a function of excitation energy are also similar. These results suggest that the B(GT) distributions of the ^{37}Cl → ^{37}Ar and ^{37}Ca → ^{37}K transitions are overall rather symmetric. This is consistent with the experimental results as seen in Fig. 8.

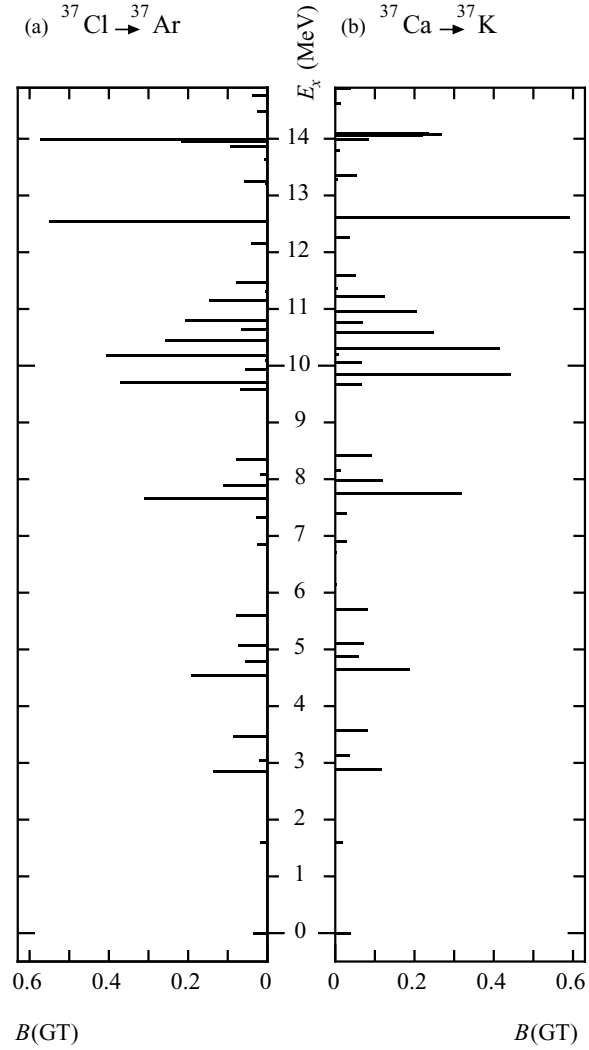

FIG. 9. The SM calculation of B(GT) values for the (a) ^{37}Cl → ^{37}Ar and (b) ^{37}Ca → ^{37}K GT transitions using the USD-INC interaction. The strengths were multiplied by a quenching factor of 0.53 to compensate for the effects of the limited model space used in the calculation.

In the SM calculation, shown in Fig. 9, the B(GT) values are almost the same within small differences of 0.03 up to $E_x = 13.9$ MeV. This SM calculation suggests that isospin symmetry is mainly preserved. In the region of 13.9–14.1 MeV, where the SM calculation shows a high level density, considerably different B(GT) strengths are predicted for the ^{37}Cl → ^{37}Ar and ^{37}Ca → ^{37}K transitions. In general, an eigenstate strongly couples with neighboring states within an energy window of $\Delta E_x \approx 100$ keV if the J^π values are the same. Therefore, a small isospin-breaking force can change significantly the B(GT) distributions of mirror nuclei [20,24]. In addition, different Coulomb energies in mirror nuclei can create fluctuations of the excitation energies from a few dozen to a few hundred keV. Such energy fluctuations can also break the symmetry of the B(GT) distribution in mirror nuclei.

In the present experiment, we find that the level density of GT states above $E_x = 5.1$ MeV is very high. Therefore, it is expected that many GT states mix with the neighboring

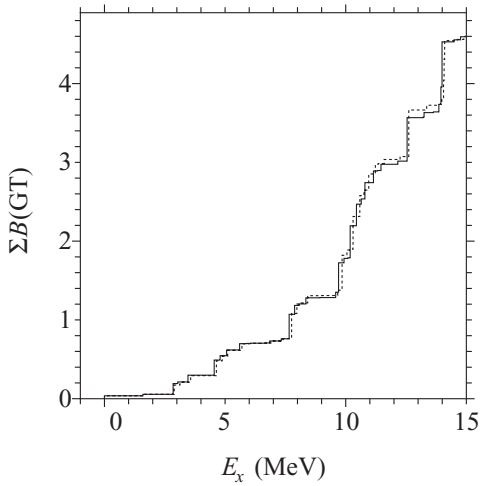

FIG. 10. Cumulative sums of the GT transition strengths calculated by the SM code OXBASH using the USD-INC interaction. The solid and dotted lines represent the ^{37}Cl → ^{37}Ar and ^{37}Ca → ^{37}K transitions, respectively. The strengths were multiplied by the quenching factor of 0.53.

states having the same J^π. This can cause the differences in the fine structures of the B(GT) distributions of ^{37}Cl → ^{37}Ar and ^{37}Ca → ^{37}K transitions. In the energy region of E_x = 0–8.65 MeV, the number of GT states observed in the ^{37}Cl(^{3}He, t)^{37}Ar reaction was 38. On the other hand, 50 states were observed in the ^{37}Ca → ^{37}K β decay in the same energy region. This discrepancy may be due to the limited energy resolution of the ^{37}Cl(^{3}He, t)^{37}Ar experiment. However, it is rather clear that the fine structures are different in ^{37}Ar and ^{37}K. The isospin-asymmetry interaction $\mathcal{H}_{\rm IA}$ was studied in Ref. [20]. The empirical $\mathcal{H}_{\rm IA}$ value was 4.8 keV. This suggests that the fragmentation of the B(GT) values in mirror nuclei can be different even if the isospin-asymmetry interaction is small. Different B(GT) distributions between mirror nuclei were also observed in ^{41}K and ^{41}Ca [14,24]. In the case of ^{41}K and ^{41}Ca, the isospin-asymmetry interaction $\mathcal{H}_{\rm IA}$ of ∼8 keV was deduced.

In the excitation energy region below 5.1 MeV, the level density is small, as can be seen in Fig 7. Therefore, the isospin symmetry of the B(GT) strengths should be well maintained. However, the B(GT) strengths observed in the ^{37}Cl(^{3}He, t)^{37}Ar study are different compared to the B(GT) values in the ^{37}Ca → ^{37}K β-decay measurement. Particularly the 2.80-, 3.17-, and 3.60-MeV states in ^{37}Ar obviously have different strengths from those of the corresponding states in ^{37}K. Watson *et al.* studied the ground-state to ground-state transitions in p-shell and sd-shell nuclei by comparing the (p, n) reaction and β decay [40,41]. They found that the proportionality of the (p, n) cross sections to the B(GT) values for the $j_< \rightarrow j_<$ transitions was uncertain by as much as 40%. Zegers *et al.* [42] studied the ^{13}C(g.s.) → ^{13}N(g.s.) GT transition via the ^{13}C(^{3}He, t)^{13}N reaction in conjunction with the DWBA calculation. They concluded that the proportionality breaking observed in the the (^{3}He, t) reaction for the ^{13}C(g.s.) → ^{13}N(g.s.) transition is caused by the interference of the tensor τ component in the effective

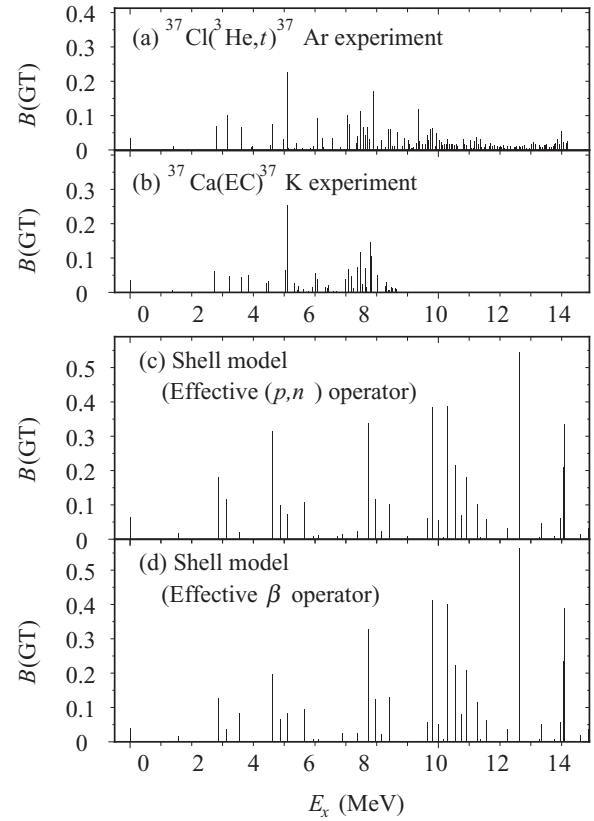

FIG. 11. Comparison of the empirical and the SM B(GT) data: (a) the B(GT) values obtained by the present ^{37}Cl(^{3}He, t)^{37}Ar study, (b) the B(GT) values obtained by the ^{37}Ca →^{37}K measurement [20], (c) the SM calculations using the USD interaction without isospin-violating forces and using the effective (p, n) operator, and (d) the SM calculations on the USD interaction without isospin-violating forces and using the effective β operator.

^{3}He-nucleon interaction. From the analogy of the $j_< \rightarrow j_<$ transition, it is expected that the tensor τ component also affects the low-lying states of the ^{37}Cl → ^{37}Ar transitions. We will discuss the effect of the tensor τ component in the ^{3}He-nucleon interaction also in Sec. IV B.

B. Strengths predicted by shell-model calculation

In Fig. 11, the B(GT) distributions of the ^{37}Cl(^{3}He, t)^{37}Ar and the ^{37}Ca → ^{37}K β-decay measurements and the theoretical results using the SM calculations with the USD interaction are compared. In the SM calculations, the effective (p, n) and β operators [38,40,44] were applied to the ^{37}Cl → ^{37}Ar and the ^{37}Ca → ^{37}K transitions, respectively. These operators effectively compensate for the limited model space of the USD interaction and result in the reduction of the strengths. In the effective operators the tensor τ components are included in addition to the predominant $\sigma\tau$ components. Especially, the effective (p, n) operator has a strong tensor τ component. Therefore, the B(GT) values produced by the SM calculation are not the pure GT strengths in terms of the $\sigma\tau$ operator. Zegers *et al.* pointed out that the strong tensor τ component observed in the (p, n) cross section for the GT state mainly

TABLE V. Comparison of the B(GT) strengths deduced from the ^{37}Cl(^{3}He, t)^{37}Ar measurements and the SM calculation for transitions to low-lying states. In the SM calculation the USD interaction and the effective (p, n) operator were used.

Experiment		SM calculation		$2J^\pi$
E_x (MeV)	B(GT)	E_x (MeV)	B(GT)	
0.0	0.0348	0.0	0.0656	3
1.410	0.009	1.585	0.0174	1
2.795	0.069	2.884	0.1809	5
3.167	0.102	3.112	0.1161	5
3.598	0.065	3.539	0.0208	3
4.986[a]	0.088	4.883[a]	0.0994	3

[a]IAS.

originated from the tensor τ component coexisting with the $\sigma\tau$ component in the nucleon-nucleon interaction [42]. At present we use the (p, n) operator to evaluate the effect of the strong tensor τ component in the ^{3}He-nucleon interaction.

Compared with the experimental spectra, the clusterings of the strengths at 2.5–4, 4–5.5, and 6.7–9.2 MeV are well reproduced. The similarity suggests that the SM calculations reproduce the gross features up to about $E_x = 10$ MeV. As shown in Table V, the lowest five levels up to 3.54 MeV and the IAS are consistent with the levels predicted by the SM calculations. Above 4 MeV the number of levels predicted by the SM calculations is much smaller compared to that from the experiment. This suggests that the model space used in the SM calculation is not large enough to reproduce the fragments.

Comparing Fig. 11(c) and 11(d), one sees that the strength distributions up to $E_x = 5$ MeV are different. In the SM calculation the strong tensor τ component included in the effective (p, n) operator produced a different distribution from that of β decay. It is expected that the strong tensor τ component in the ^{3}He-nucleon interaction in the ^{37}Cl(^{3}He, t)^{37}Ar reaction also changes the distribution. On the other hand, the distributions above $E_x = 5$ MeV are similar. This indicates that the tensor τ component little affects the transition strength in the highly excited energy region, perhaps due to the fact that the tensor τ operator produces a larger value for the $j_< \rightarrow j_<$ transition than for the $j_> \rightarrow j_<$ transition.

In order to see the differences of the gross features of the strength distributions between the empirical data and the SM calculation, we compared the cumulative sums of the B(GT) strengths as a function of excitation energy for the experiment and the SM, as shown in Fig. 12. The experimental cumulative sum without the continuum and the theoretical cumulative sum show rather good agreement up to about 10 MeV. Above 10 MeV, however, the SM calculation overestimates the experimental strength. The integrated value of the empirical B(GT) values up to $E_x = 14.2$ MeV is 3.36 ± 0.13 without the continuum. On the other hand, the integrated value of B(GT) from the SM calculation is 4.6. Although the inclusion of the continuum in the experimental data results in a cumulative sum similar to that of the SM calculation, the continuum can contain components other than $L = 0$.

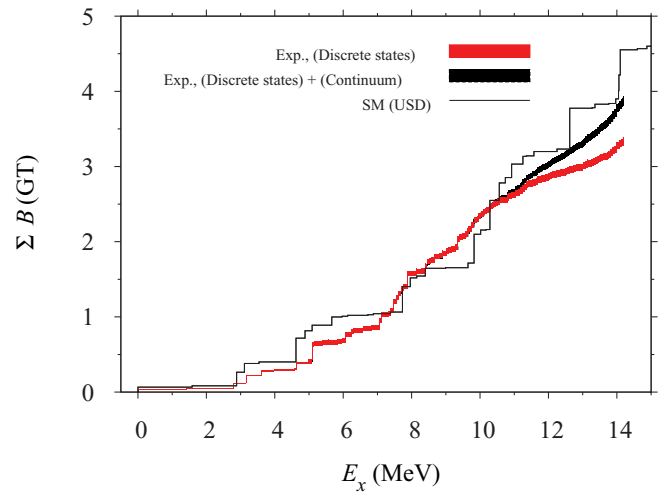

FIG. 12. (Color online) Comparison of cumulative sums of B(GT) values for ^{37}Cl $\rightarrow$ ^{37}Ar transitions of the experiment and the SM calculation. The gray (red online) and black bands show the data without and with the continuum, respectively. The solid line represents the SM calculation based on the USD interaction with the effective (p, n) operator. The cumulative sum of the SM calculation is reduced by multiplying by the quenching factor of 0.53.

C. Solar-neutrino capture rates

As mentioned, ^{37}Cl has been used as a solar-neutrino detector using the ^{37}Cl(ν, e^-)^{37}Ar reaction that is dominantly caused by the GT transition. ^{8}B β decay with high neutrino energies and high fluxes is the most important solar-neutrino source to be measured by a ^{37}Cl detector. The solar-neutrino absorption cross section depends not only on the B(GT) distribution in ^{37}Ar but also on the neutrino energy distribution. With improvements of both data, the neutrino absorption cross section of ^{37}Cl has been updated many times [3,46]. The latest value of the ^{8}B neutrino cross section is $\sigma_{\rm Cl} = (1.14 \pm 0.037) \times 10^{-42}$cm^2 [3], which was based on the ^{37}Cl$(p, n)^{37}$Ar and ^{37}Ca β-decay data. In order to see the effects of the new B(GT) data of this study, we recalculated the ^{8}B neutrino cross section.

The ^{8}B neutrino spectrum is extracted from the measurement of two-α-particle emission via ^{8}B$(\beta^+)^8$Be(2α). Bahcall *et al.* systematically studied the ^{8}B neutrino spectrum by using available empirical data and new theoretical calculations [46]. Subsequently, Ortiz *et al.* [47] and Winter *et al.* [48] performed additional measurements of ^{8}B β decay and extracted more precise ^{8}B neutrino spectra. However, the result of Ortiz *et al.* was inconsistent with that of Winter *et al.* In this study, we separately calculate the ^{8}B neutrino cross sections for these three cases.

In calculating the neutrino cross sections, we only used the B(GT) values of the ^{37}Cl(^{3}He, t)^{37}Ar experiment from the region $E_x > 5.1$ MeV. For $E_x \leqslant 5.1$ MeV we applied the B(GT) values of the ^{37}Ca β decay reported by Kaloskamis *et al.* [20], because the B(GT) values obtained by the ^{37}Cl(^{3}He, t)^{37}Ar reaction can have large ambiguities in the region of $E_x \leqslant 5.1$ MeV. The Fermi transition strength, B(F), to the IAS at $E_x = 4.99$ MeV was assumed to be the sum rule value of 3. Combining those B(GT) values and the ^{8}B neutrino

TABLE VI. ^{8}B neutrino cross sections for different neutrino spectra. The cross section of each state is given in units of 10^{-46} cm^2. In order to calculate the ^{8}B neutrino cross sections, we used the B(GT) values of the ^{37}Cl(^{3}He, t)^{37}Ar experiment and the ^{37}Ca β-decay measurement [20] for $E_x > 5.1$ MeV and $E_x \leqslant 5.1$ MeV, respectively.

E_x	B(GT)	σ_{Cl}[a]	σ_{Cl}[b]	σ_{Cl}[c]
0.00	0.035	680(40)	690(40)	690(40)
1.41	0.0078	101(5)	103(5)	103(5)
2.79	0.062	510(70)	520(80)	520(80)
3.17	0.048	350(90)	350(90)	350(90)
3.6	0.0448	270(8)	278(8)	276(8)
3.94	0.0507	265(8)	273(8)	271(8)
3.98	0.0064	33.1(15)	34.1(16)	33.8(16)
4.57	0.0258	103(3)	106(3)	105(3)
4.63	0.0339	131(4)	136(4)	135(4)
4.98	0.06	6400(170)[d]	6600(180)[d]	6600(180)[d]
5.10	0.226	710(30)	730(30)	720(30)
5.15	0.0040	12(3)	12(3)	12(3)
5.34	0.0036	9.9(14)	10.3(15)	10.2(15)
5.40	0.0178	48(3)	49(3)	49(3)
5.58	0.0032	7.8(14)	8.1(14)	8.0(14)
5.85	0.0035	7.4(12)	7.7(13)	7.6(13)
5.96	0.0114	22(2)	23(2)	23(2)
6.07	0.092	170(70)	180(70)	180(70)
6.25	0.035	59(4)	62(4)	61(4)
6.29	0.0066	11(2)	11(2)	11(2)
6.58	0.034	47(3)	49(3)	48(3)
6.83	0.0075	8.9(16)	9.4(17)	9.3(16)
7.05	0.100	103(4)	109(4)	107(4)
7.13	0.074	73(3)	77(3)	76(3)
7.33	0.0180	15.5(14)	16.4(15)	16.1(15)
7.38	0.040	34(2)	36(2)	35(2)
7.47	0.113	88(3)	93(4)	91(4)
7.56	0.065	48(2)	51(2)	50(2)
7.62	0.041	28.7(16)	30.3(17)	29.8(17)
7.69	0.067	44(2)	47(2)	46(2)
7.77	0.031	19.5(15)	20(16)	20(15)
7.89	0.170	98(4)	104(4)	102(4)
8.03	0.0099	5.1(10)	5.5(11)	5.4(11)
8.15	0.028	13.3(12)	14.2(13)	13.9(13)
8.28	0.0074	3.2(3)	3.4(4)	3.3(4)
8.40	0.058	22.7(10)	24.2(11)	23.7(10)
8.45	0.059	21.8(9)	23.4(10)	22.9(10)
8.52	0.0107	3.8(4)	4.0(4)	3.9(4)
8.58	0.0093	3.1(5)	3.3(5)	3.3(5)
8.66	0.051	15.9(7)	17.1(8)	16.8(7)
8.83	0.0098	2.7(3)	2.9(3)	2.8(3)
8.91	0.033	8.2(6)	8.9(6)	8.7(6)

[a]For the neutrino spectrum by Bahcall *et al.* [46].
[b]For the neutrino spectrum by Ortiz *et al.* [47].
[c]For the neutrino spectrum by Winter *et al.* [48].
[d]The cross section for the Fermi transition is included.

TABLE VII. The same as Table VI, but for the higher excited states.

E_x	B(GT)	σ_{Cl}[a]	σ_{Cl}[b]	σ_{Cl}[c]
9.02	0.026	6.0(5)	6.4(6)	6.3(6)
9.08	0.0160	3.4(3)	3.7(3)	3.6(3)
9.14	0.0053	1.1(3)	1.2(3)	1.1(3)
9.17	0.0049	1.0(2)	1.0(3)	1.0(3)
9.21	0.0060	1.14(16)	1.23(18)	1.20(17)
9.29	0.0194	3.4(3)	3.7(3)	3.6(3)
9.35	0.117	19.3(8)	21.0(9)	20.5(8)
9.40	0.024	3.7(4)	4.1(4)	4.0(4)
9.49	0.0152	2.2(2)	2.4(2)	2.3(2)
9.58	0.0148	1.9(2)	2.1(2)	2.1(2)
9.64	0.041	5.1(5)	5.5(5)	5.4(5)
9.67	0.027	3.2(5)	3.5(5)	3.4(5)
9.75	0.060	6.6(4)	7.2(4)	7.0(4)
9.82	0.063	6.3(6)	6.9(7)	6.7(6)
9.91	0.0091	0.83(16)	0.92(18)	0.89(18)
9.96	0.047	4.1(2)	4.5(3)	4.4(3)
10.03	0.0278	2.22(17)	2.44(18)	2.37(18)
10.10	0.022	1.6(2)	1.8(3)	1.7(3)
10.14	0.013	8.8(2)	9.7(2)	9.4(2)
10.19	0.0162	1.07(11)	1.18(12)	1.14(12)
10.26	0.017	1.0(4)	1.1(4)	1.1(4)
10.29	0.031	1.8(4)	2.0(4)	1.9(4)
10.36	0.0166	0.89(10)	0.99(11)	0.95(11)
10.41	0.016	0.81(10)	0.90(12)	0.87(11)
10.45	0.016	0.77(10)	0.85(11)	0.82(10)
10.52	0.0139	0.61(7)	0.68(8)	0.65(8)
10.58	0.0168	0.68(7)	0.75(8)	0.73(8)
10.63	0.0092	0.35(7)	0.39(7)	0.37(7)
10.81	0.029	0.9(2)	0.9(3)	0.9(3)
10.83	0.016	0.5(2)	0.5(3)	0.5(3)
10.93	0.0125	0.31(5)	0.35(5)	0.34(5)
11.03	0.028	0.60(5)	0.68(5)	0.66(5)
11.07	0.0043	0.09(3)	0.10(3)	0.09(3)
11.13	0.0033	0.06(3)	0.07(3)	0.07(3)
11.17	0.026	0.44(6)	0.50(7)	0.48(7)
11.23	0.037	0.58(4)	0.66(4)	0.63(4)
11.31	0.0154	0.21(3)	0.24(3)	0.23(3)
11.37	0.031	0.39(3)	0.45(3)	0.42(3)
11.41	0.008	0.10(2)	0.11(3)	0.11(3)
11.48	0.0070	0.072(16)	0.083(18)	0.079(17)
11.53	0.0166	0.16(18)	0.18(20)	0.17(19)
11.65	0.012	0.089(17)	0.102(19)	0.097(18)
11.68	0.019	0.139(17)	0.16(2)	0.151(19)

[a]For the neutrino spectrum by Bahcall *et al.* [46].
[b]For the neutrino spectrum by Ortiz *et al.* [47].
[c]For the neutrino spectrum by Winter *et al.* [48].

spectra [46–48], we calculated the neutrino cross sections. The obtained cross sections are listed in Tables VI, VII, and VIII. Only uncertainties of the cross sections originating from the uncertainties of the B(GT) values are shown. If we take the uncertainties of the neutrino spectra into account, the uncertainties of the cross sections can become larger. It is possible that the uncertainties of the total ^{8}B neutrino cross sections amount to more than 5% if the ambiguities of the ^{8}B neutrino spectra are included. In addition, if forbidden transitions are included, the total cross sections may increase by a few percent [49]. The ^{8}B neutrino cross sections obtained in this work and those given by Bahcall [46] are in agreement within uncertainties.

TABLE VIII. The same as Table VI, but for the higher excited states. The total cross sections are given in units of 10^{-42} cm^2.

E_x	B(GT)	σ_{Cl}[a]	σ_{Cl}[b]	σ_{Cl}[c]
11.74	0.010	0.065(16)	0.075(18)	0.071(17)
11.81	0.012	0.070(11)	0.080(13)	0.075(12)
11.93	0.0092	0.042(8)	0.048(10)	0.045(9)
11.97	0.0061	0.025(12)	0.029(14)	0.028(13)
12.00	0.011	0.042(10)	0.049(11)	0.045(10)
12.05	0.0064	0.022(6)	0.026(7)	0.024(7)
12.10	0.012	0.039(7)	0.045(8)	0.041(7)
12.16	0.005	0.013(7)	0.015(8)	0.014(8)
12.24	0.011	0.025(5)	0.029(5)	0.027(5)
12.34	0.011	0.021(5)	0.024(6)	0.022(5)
12.46	0.008	0.012(3)	0.014(4)	0.013(4)
12.49	0.008	0.010(3)	0.011(4)	0.010(3)
12.54	0.011	0.012(3)	0.014(3)	0.013(3)
12.58	0.003	0.003(3)	0.003(3)	0.003(3)
12.62	0.010	0.009(2)	0.011(2)	0.096(2)
12.66	0.007	0.0057(17)	0.0067(20)	0.0061(19)
12.73	0.009	0.0064(15)	0.0076(17)	0.0068(16)
12.80	0.012	0.0070(12)	0.0082(15)	0.0072(13)
12.85	0.004	0.0021(10)	0.0025(12)	0.0022(11)
12.96	0.004	0.0016(10)	0.0019(12)	0.0017(10)
13.01	0.017	0.0053(8)	0.0062(9)	0.0054(8)
13.08	0.023	0.0059(8)	0.0070(10)	0.0062(9)
13.14	0.015	0.0033(6)	0.0039(7)	0.0034(6)
13.27	0.013	0.0019(4)	0.0022(5)	0.0019(4)
13.31	0.008	0.0010(4)	0.0011(4)	0.0009(4)
13.37	0.008	0.0008(3)	0.0009(3)	0.0009(3)
13.44	0.014	0.0012(4)	0.0014(5)	0.0012(4)
13.48	0.014	0.0010(3)	0.0012(4)	0.0010(3)
13.52	0.016	0.0010(3)	0.0012(3)	0.0009(3)
13.60	0.008	0.00037(13)	0.00043(14)	0.00033(11)
13.66	0.009	0.00034(11)	0.00039(13)	0.00032(10)
13.72	0.011	0.00035(11)	0.00040(13)	0.00031(10)
13.77	0.017	0.00044(10)	0.00050(11)	0.00040(9)
13.82	0.019	0.00042(7)	0.00047(7)	0.00035(6)
13.87	0.030	0.00052(6)	0.00058(7)	0.00046(6)
13.93	0.016	0.00023(5)	0.00026(5)	0.00019(4)
14.00	0.053	0.00058(5)	0.00064(5)	0.00042(3)
14.07	0.022	0.00019(2)	0.00020(3)	0.000141(19)
14.14	0.020	0.00012(2)	0.00013(3)	0.000082(16)
14.19	0.026	0.000124(18)	0.00014(2)	0.000073(11)
Total		1.08(2)	1.12(2)	1.10(2)

[a]For the neutrino spectrum by Bahcall *et al.* [46].
[b]For the neutrino spectrum by Ortiz *et al.* [47].
[c]For the neutrino spectrum by Winter *et al.* [48].

V. SUMMARY

We performed a high-resolution ^{37}Cl(^{3}He, t)^{37}Ar experiment at an incident energy of 420 MeV/nucleon and a spectrometer angle of 0°. By using the proportionality between differential cross sections and B(GT) values, we extracted the B(GT) values for the transitions from the g.s. of ^{37}Cl to the excited states in ^{37}Ar. In order to determine the absolute B(GT) values, we normalized the counts integrated over the excitation-energy region of $E_x = 5.93$–8.15 MeV to the B(GT) values of the mirror-symmetric ^{37}Ca $\rightarrow$ ^{37}K transitions obtained from previous β-decay measurements. Comparing the B(GT) distributions of the ^{37}Cl $\rightarrow$ ^{37}Ar to the mirror transitions of ^{37}Ca $\rightarrow$ ^{37}K, we found that the overall distributions are similar. However, the fine structures are not necessarily in agreement. The SM calculations suggest that, in the region where the level density is high, a small change in the Coulomb force can make a large difference in the B(GT) distributions of ^{37}Cl $\rightarrow$ ^{37}Ar and ^{37}Ca $\rightarrow$ ^{37}K transitions. In fact the measured level densities above $E_x = 5.1$ MeV in ^{37}Ar and ^{37}K are very high. Therefore, it is inferred that the different B(GT) distributions are due to the different configurations of the analog states of ^{37}Ar and ^{37}K.

There are differences even for low-lying states where the level density is low. This suggests that the proportionality between differential cross sections and B(GT) values are broken by up to 40% due to the ($j_< \rightarrow j_<$) nature of the transition.

By using the measured B(GT) values, we calculated the neutrino absorption cross section. The total absorption cross sections for the ^{8}B neutrino based on the neutrino spectra of Ref. [46], Ref. [47], and Ref [48] were 1.08, 1.12, and 1.10 in units of 10^{-42} cm^2, respectively. We found that the obtained ^{8}B neutrino absorption cross section was in agreement with the previous data of Ref. [46]. This suggests that the effect of the new B(GT) data at $E_x > 8.65$ MeV was small for the ^{8}B neutrino absorption cross section.

ACKNOWLEDGMENTS

The (^{3}He, t) experiment was performed at RCNP, Osaka University, under the Experimental Program E158. We thank the RCNP staff for their efforts in running this experiment. We would like to acknowledge many helpful discussions with Dr. B. A. Brown, Dr. R. G. T. Zegers, and Dr. T. Suzuki. We are grateful to Dr. A. García for sending the ^{8}B neutrino spectrum. This work was supported in part by MEXT, Japan, under Grant No. 18540270.

[1] R. Davis, D. S. Harmer, and K. C. Hoffman, Phys. Rev. Lett. **20**, 1205 (1968).
[2] J. N. Bahcall, N. A. Bahcall, and G. Shaviv, Phys. Rev. Lett. **20**, 1209 (1968).
[3] B. T. Cleveland, T. Daily, R. Davis, J. R. Distel, K. Lande, C. K. Lee, P. S. Wildenhain, and J. Ullman, Astrophys. J. **496**, 505 (1998).
[4] J. C. Hardy and R. I. Verrall, Phys. Rev. Lett. **13**, 764 (1964).
[5] P. L. Reeder, A. M. Poskanzer, and R. A. Esterlund, Phys. Rev. Lett. **13**, 767 (1964).
[6] A. M. Poskanzer, R. McPherson, R. A. Esterlund, and P. L. Reeder, Phys. Rev. **152**, 995 (1966).
[7] R. G. Sextro, R. A. Gough, and J. Cerny, Nucl. Phys. A **234**, 130 (1974).
[8] J. Rapaport *et al.*, Phys. Rev. Lett. **47**, 1518 (1981).

[9] T. N. Taddeucci, C. A. Goulding, T. A. Carey, R. C. Byrd, C. D. Goodman, C. Gaarde, J. Larsen, D. Horen, J. Rapaport, and E. Sugarbaker, Nucl. Phys. A **469**, 125 (1987).
[10] Y. Fujita *et al*., Phys. Rev. C **59**, 90 (1999).
[11] Y. Fujita *et al*., Phys. Rev. C **66**, 044313 (2002).
[12] Y. Fujita *et al*., Phys. Rev. C **67**, 064312 (2003).
[13] R. G. T. Zegers *et al*., Phys. Rev. C **74**, 024309 (2006).
[14] Y. Fujita, B. Rubio, and W. Gelletly, Prog. Part. Nucl. Phys. **66**, 549 (2011).
[15] E. G. Adelberger and W. C. Haxton, Phys. Rev. C **36**, 879 (1987).
[16] A. García, E. G. Adelberger, P. V. Magnus, H. E. Swanson, O. Tengblad, ISOLDE Collaboration, and D. M. Moltz, Phys. Rev. Lett. **67**, 3654 (1991).
[17] C. Iliadis, J. Höhne, F. Käppeler, J. Meissner, H. P. Trautvetter, and M. Wiescher, Phys. Rev. C **48**, R1479 (1993).
[18] P. V. Magnus, E. G. Adelberger, and N. Cabot, Phys. Rev. C **51**, 2806 (1995).
[19] W. Trinder *et al*., Nucl. Phys. A **620**, 191 (1997).
[20] N. I. Kaloskamis, A. García, S. E. Darden, E. Miller, W. Haeberli, P. A. Quin, B. P. Schwartz, E. Yacoub, and E. G. Adelberger, Phys. Rev. C **55**, 640 (1997).
[21] C. D. Goodman, Nucl. Phys. A **577**, 3c (1994).
[22] Y. Shimbara *et al*., Eur. Phys. J. A **19**, 25 (2004).
[23] Y. Fujita *et al*., Phys. Rev. C **75**, 057305 (2007).
[24] Y. Fujita *et al*., Phys. Rev. C **70**, 054311 (2004).
[25] A. Honkanen *et al*., Nucl. Phys. A **621**, 689 (1997).
[26] M. Fujiwara *et al*., Nucl. Instrum. Methods A **422**, 484 (1999).
[27] K. Hatanaka, J. Korean Phys. Soc. **54**, 1937 (2009); [http://www.rcnp.osaka-u.ac.jp/].
[28] T. Noro *et al*., RCNP Annual Report, 1991, p. 177.
[29] Y. Shimbara *et al*., Nucl. Instrum. Methods A **522**, 205 (2004).
[30] Y. Fujita, K. Hatanaka, G. P. A. Berg, K. Hosono, N. Matsuoka, S. Morinobu, T. Noro, M. Sato, K. Tamura, and H. Ueno, Nucl. Instrum. Methods B **126**, 274 (1997), and references therein.
[31] T. Wakasa *et al*., Nucl. Instrum. Methods A **482**, 79 (2002).
[32] H. Fujita *et al*., Nucl. Instrum. Methods A **484**, 17 (2002).
[33] Y. Fujita *et al*., J. Mass Spectrom. Soc. Jpn. **48**, 306 (2000).
[34] P. M. Endt, Nucl. Phys. A **521**, 1 (1990); **633**, 1 (1998), and references therein.
[35] H. Fujita *et al*., Nucl. Instrum. Methods A **469**, 55 (2001).
[36] A. Erell, J. Alster, J. Lichtenstadt, M. A. Moinester, J. D. Bowman, M. D. Cooper, F. Irom, H. S. Matis, E. Piasetzky, and U. Sennhauser, Phys. Rev. C **34**, 1822 (1986).
[37] J. Jänecke *et al*., Phys. Rev. C **48**, 2828 (1993).
[38] B. A. Brown (private communication).
[39] B. H. Wildenthal, Prog. Part. Nucl. Phys. **11**, 5 (1984), B. A. Brown and B. H. Wildenthal, Annu. Rev. Nucl. Part. Sci. **38**, 29 (1988).
[40] J. W. Watson, W. Pairsuwan, B. D. Anderson, A. R. Baldwin, B. S. Flanders, R. Madey, R. J. McCarthy, B. A. Brown, B. H. Wildenthal, and C. C. Foster, Phys. Rev. Lett. **55**, 1369 (1985).
[41] J. W. Watson and Q. Q. Du, Nucl. Phys. A **687**, 32c (2001).
[42] R. G. T. Zegers *et al*., Phys. Rev. C **77**, 024307 (2008).
[43] Y. Fujita (private communication).
[44] B. A. Brown and B. H. Wildenthal, Nucl. Phys. A **474**, 290 (1987).
[45] B. A. Brown and B. H. Wildenthal, Annu. Rev. Nucl. Part. Sci. **38**, 29 (1988).
[46] J. N. Bahcall, E. Lisi, D. E. Alburger, L. De Braeckeleer, S. J. Freedman, and J. Napolitano, Phys. Rev. C **54**, 411 (1996). The numerical data of the neutrino spectrum was obtained from [http://www.sns.ias.edu/jnb/].
[47] C. E. Ortiz, A. García, R. A. Waltz, M. Bhattacharya, and A. K. Komives, Phys. Rev. Lett. **85**, 2909 (2000).
[48] W. T. Winter *et al*., Phys. Rev. Lett. **91**, 252501 (2003).
[49] J. N. Bahcall and B. R. Holstein, Phys. Rev. C **33**, 2121 (1986).